AMORPHOUS THIN FILM GROWTH SIMULATION METHODS FOR STOCHASTIC DEPOSITION EQUATIONS*

Martin Raible, Stefan J. Linz and Peter Hänggi

Theoretische Physik I, Institut für Physik, Universität Augsburg
86135 Augsburg, Germany

(Received November 27, 2001)

Different methods for the numerical solution of a stochastic growth equation capturing the essence of amorphous thin film growth are presented and compared. We show numerically that the finite difference approximation and the spectral Galerkin method yield the same results within the same accuracy and roughly comparable computation time. We also explain how stochastic field equations can be solved using finite element approximations.

PACS numbers: 02.60.Cb, 02.60.Lj, 02.50.Ey, 68.55.–a

1. Introduction

The topic of formation and spatio-temporal evolution of surfaces generated by deposition processes has recently developed into a highly active research area of statistical physics (see Ref. [1]). Specifically, the growth process of the surface of the deposited film, as it appears in molecular beam epitaxy or physical vapor deposition experiments, is determined by the competition between roughening due to the deposition of particles and smoothing due to surface diffusion effects [2–6]. Experimental studies on *amorphous films* deposited by electron beam evaporation have revealed the formation of moundlike surface structures on a mesoscopic length scale [7–10]. This indicates that continuum models based on *stochastic* field equations of the form

$$\partial_t H = G(H) + \eta + F\,, \tag{1}$$

can serve as a useful tool for the understanding of the growth dynamics. Here, $H(\vec{x},t)$ represents the height of the surface above a given substrate position $\vec{x}$ at time t, as shown in Fig. 1. $G(H)$ represents a functional of the spatial derivatives of the height function H and includes all surface

* Presented at the XIV Marian Smoluchowski Symposium on Statistical Physics, Zakopane, Poland, September 9–14, 2001.

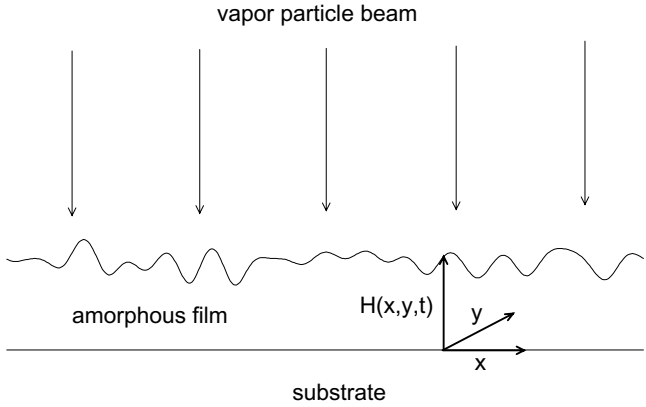

Fig. 1. Sketch of the vapor deposition of an amorphous film on a substrate.

relaxation processes and possible growth instabilities. F denotes the mean deposition rate, and η quantifies the deposition noise that represents the fluctuations of the deposition flux around its mean F. These fluctuations are assumed to be Gaussian white, *i.e.*

$$\langle \eta(\vec{x},t)\rangle = 0\,, \quad \langle \eta(\vec{x},t)\eta(\vec{y},t')\rangle = 2D\delta^2(\vec{x}-\vec{y})\delta(t-t')\,, \tag{2}$$

where the brackets denote ensemble averaging and D the fluctuation strength. A transformation into a frame comoving with the deposition rate F, $h(\vec{x},t) = H(\vec{x},t) - Ft$, yields a corresponding evolution equation for the height profile $h(\vec{x},t)$

$$\partial_t h = G(h) + \eta\,. \tag{3}$$

A comparison with experimental data for amorphous $Zr_{65}Al_{7.5}Cu_{27.5}$ films deposited by electron beam evaporation has recently evidenced a good quantitative agreement between numerical solutions of the model equation [11–13]

$$\partial_t h = a_1\nabla^2 h + a_2\nabla^4 h + a_3\nabla^2(\nabla h)^2 + a_4(\nabla h)^2 + \eta \tag{4}$$

and experimental measurements up to the largest, experimentally observed layer thickness of 480 nm [11]. Moske [14] had already suggested the equation $\partial_t h = a_2\nabla^4 h + a_3\nabla^2(\nabla h)^2 + \eta$ as a model for amorphous film growth. This equation, however, is not able to capture the experimentally observed pattern-forming surface structure. Based on microscopic models [12–14] for the governing surface relaxation mechanisms, it has been found that the coefficients a_1, a_2, and a_3 in Eq. (4) are negative, whereas a_4 is positive. The term $a_1\nabla^2 h$ with negative a_1 represents in combination with the term $a_2\nabla^4 h$ the same growth instability as in the Kuramoto–Sivashinsky equation, that is known to trigger the formation of moundlike surface structures. For a mathematical proof of existence of a solution of Eq. (4) in the one-dimensional case we refer to Ref. [15].

Surface growth equations of the form (3) and (4) are usually solved on a quadratic area $[0, L]^2$ subject to periodic boundary conditions. The initial state is given by $h(\vec{x}, 0) = 0$, corresponding to an initially flat substrate. In order to compare the solutions of such stochastic growth equations with experimental results, experimentally accessible statistical quantities have to be introduced. The correlation length $R_c(t)$ and the surface roughness $w(t)$ are such characteristic quantities and are determined by the height–height correlation function

$$C(r,t) = \left\langle \left\langle \frac{1}{L^2} \int d^2x \, [h(\vec{x},t) - \overline{h}(t)][h(\vec{x}+\vec{r},t) - \overline{h}(t)] \right\rangle \right\rangle_{|\vec{r}|=r} , \qquad (5)$$

where $\overline{h}(t) = (1/L^2) \int d^2x \, h(\vec{x}, t)$ denotes the spatial average of the height, and $\langle\langle \ldots \rangle\rangle_{|\vec{r}|=r}$ denotes the combined ensemble and radial average. Specifically, $R_c(t)$ is given by the radius r of the first maximum of $C(r, t)$ occurring at nonzero values of r and the square of the surface roughness results from taking the limit $r = 0$ in $C(r, t)$, *i.e.* $w^2(t) = C(0, t)$. The quantities $w(t)$ and $R_c(t)$ characterize the typical height and periodicity length scales of the moundlike surface structure.

The aim of this paper is twofold. First, using the specific example of Eq. (4), we present three different methods to numerically solve stochastic field equations: the finite difference method, the spectral Galerkin method, and the finite element method. Here, particular focus is put on the incorporation of the stochastic contributions in these numerical schemes. Second, by specific calculations of the correlation length $R_c(t)$ and the surface roughness $w(t)$ arising from Eq. (4), we compare the numerical efficiency of the finite difference and the spectral Galerkin method. The presented schemes can also serve as a guide for the numerical solution of stochastic growth equations with different functional structure.

2. Finite difference method

The most common method to numerically integrate stochastic field equations such as Eq. (3) is based on a direct spatio-temporal discretization on a cubic grid with a spatial lattice constant $\Delta x = \Delta y = L/N$ and a time step Δt_n. The finite difference discretization of the general form (3) of a stochastic deposition equation reads

$$h_{i,j}^{(n+1)} = h_{i,j}^{(n)} + \Delta t_n G_{i,j}[h_{k,l}^{(n)}] + P_n \xi_{i,j}^{(n)} \qquad (6)$$

with

$$P_n = \sqrt{24 D \Delta t_n / (\Delta x)^2} \, . \qquad (7)$$

Here, $h_{i,j}^{(n)}$ denotes the spatial average of the height function h at the time t_n on one of N^2 squares of a quadratic lattice on $[0,L]^2$, *i.e.*

$$h_{i,j}^{(n)} = \frac{1}{(\Delta x)^2} \int\limits_{(i-1/2)\Delta x}^{(i+1/2)\Delta x} dx \int\limits_{(j-1/2)\Delta x}^{(j+1/2)\Delta x} dy\, h(x,y,t_n) \tag{8}$$

with $i,j \in \mathbb{Z}$. The quantity $\Delta t_n = t_{n+1} - t_n$ denotes the size of the generally variable time step, and the quantities $\xi_{i,j}^{(n)}$ are independent random numbers taken from a uniform distribution between $-1/2$ and $1/2$. $G_{i,j}[h_{k,l}^{(n)}]$ is a suitable finite difference approximation of the functional $G(h)$ at the time t_n and at the position $(i\Delta x, j\Delta y)$. Different authors [16–18] have used finite difference schemes of the type (6) in order to numerically solve the Kardar–Parisi–Zhang-equation $\partial_t h = \nu\nabla^2 h + \lambda(\nabla h)^2 + \eta$ [19]. The stochastic contribution $P_n\xi_{i,j}^{(n)}$ on the RHS of Eq. (6) represents the noise η integrated over the time interval $[t_n, t_n + \Delta t_n]$ and spatially averaged on the same square around the point $(i\Delta x, j\Delta y)$ as in the definition of $h_{i,j}^{(n)}$, Eq. (8),

$$q_{i,j}^{(n)} = \frac{1}{(\Delta x)^2} \int\limits_{t_n}^{t_n+\Delta t_n} dt \int\limits_{(i-1/2)\Delta x}^{(i+1/2)\Delta x} dx \int\limits_{(j-1/2)\Delta x}^{(j+1/2)\Delta x} dy\, \eta(x,y,t)\,. \tag{9}$$

Here, $q_{i,j}^{(n)}$ and the stochastic term $P_n\xi_{i,j}^{(n)}$ in the numerical scheme (6) have the same statistical mean $\langle q_{i,j}^{(n)}\rangle = \langle P_n\xi_{i,j}^{(n)}\rangle = 0$ and the same variance $\langle (q_{i,j}^{(n)})^2\rangle = \langle (P_n\xi_{i,j}^{(n)})^2\rangle = 2D\Delta t_n/(\Delta x)^2$. In practice, it is not necessary to replace the terms $P_n\xi_{i,j}^{(n)}$ by the normally distributed random numbers $q_{i,j}^{(n)}$ because their first and second moments are equal and their higher moments are small, *i.e.* of the order $\mathcal{O}(\Delta t_n^2)$. This argument originates from the numerical integration theory of stochastic ordinary differential equations [20]. It can also be used here because, after fixing the noise strength D together with all other possible coefficients of Eq. (3) including the lattice spacing Δx and then keeping only the size of the time step Δt_n variable, Eq. (6) constitutes an explicit Euler scheme for a system of stochastic ordinary differential equations.

In order to derive a finite difference approximation of Eq. (4) we decompose this equation into the system of equations

$$\partial_t h = \nabla^2 w + a_3\nabla^2 v + a_4 v + \eta\,, \tag{10}$$

$$w = a_1 h + a_2\nabla^2 h\,, \tag{11}$$

$$v = (\nabla h)^2\,. \tag{12}$$

By using central difference approximations in space and an explicit Euler scheme in time we obtain the numerical procedure

$$\begin{aligned} h_{i,j}^{(n+1)} &= h_{i,j}^{(n)} + \frac{\Delta t_n}{(\Delta x)^2}\left[w_{i+1,j}^{(n)} + w_{i-1,j}^{(n)} + w_{i,j+1}^{(n)} + w_{i,j-1}^{(n)} - 4w_{i,j}^{(n)}\right] \\ &\quad + \frac{\Delta t_n}{(\Delta x)^2} a_3 \left[v_{i+1,j}^{(n)} + v_{i-1,j}^{(n)} + v_{i,j+1}^{(n)} + v_{i,j-1}^{(n)} - 4v_{i,j}^{(n)}\right] \\ &\quad + \Delta t_n a_4 v_{i,j}^{(n)} + P_n \xi_{i,j}^{(n)} , \qquad (13) \end{aligned}$$

$$w_{i,j}^{(n)} = a_1 h_{i,j}^{(n)} + \frac{a_2}{(\Delta x)^2}\left[h_{i+1,j}^{(n)} + h_{i-1,j}^{(n)} + h_{i,j+1}^{(n)} + h_{i,j-1}^{(n)} - 4h_{i,j}^{(n)}\right], \qquad (14)$$

$$\begin{aligned} v_{i,j}^{(n)} &= \frac{1}{3(\Delta x)^2}\left[\left(h_{i+1,j}^{(n)} - h_{i,j}^{(n)}\right)^2 + \left(h_{i+1,j}^{(n)} - h_{i,j}^{(n)}\right)\left(h_{i,j}^{(n)} - h_{i-1,j}^{(n)}\right)\right. \\ &\quad + \left(h_{i,j}^{(n)} - h_{i-1,j}^{(n)}\right)^2 + \left(h_{i,j+1}^{(n)} - h_{i,j}^{(n)}\right)^2 \\ &\quad \left. + \left(h_{i,j+1}^{(n)} - h_{i,j}^{(n)}\right)\left(h_{i,j}^{(n)} - h_{i,j-1}^{(n)}\right) + \left(h_{i,j}^{(n)} - h_{i,j-1}^{(n)}\right)^2\right]. \qquad (15) \end{aligned}$$

This numerical scheme is of the form (6). An alternative finite difference approximation of $v = (\nabla h)^2$ would read

$$v_{i,j}^{(n)} = \frac{1}{4(\Delta x)^2}\left[\left(h_{i+1,j}^{(n)} - h_{i-1,j}^{(n)}\right)^2 + \left(h_{i,j+1}^{(n)} - h_{i,j-1}^{(n)}\right)^2\right]. \qquad (16)$$

However, our numerical simulations have revealed that in the time range that is dominated by the nonlinear terms of Eq. (4) the computational procedure (13)–(15) possesses a better numerical stability than the numerical scheme composed of equations (13), (14), and (16).

As a specific application, we have solved Eq. (4) using the finite difference approximation (13)–(15). The chosen parameters were $L = 200$, $a_1 = -0.1045$, $a_2 = -0.4044$, $a_3 = -0.13$, $a_4 = 0.07$, and $D = 0.022$. These parameters are up to a rescaling of time in agreement with the parameters that resulted from a comparison with the experiments [11]. In Fig. 2, we present the resulting surface roughness $w(t)$ and correlation length $R_c(t)$ for $N^2 = 200^2$ and $N^2 = 400^2$ grid points. Their difference is not larger than 3.6%.

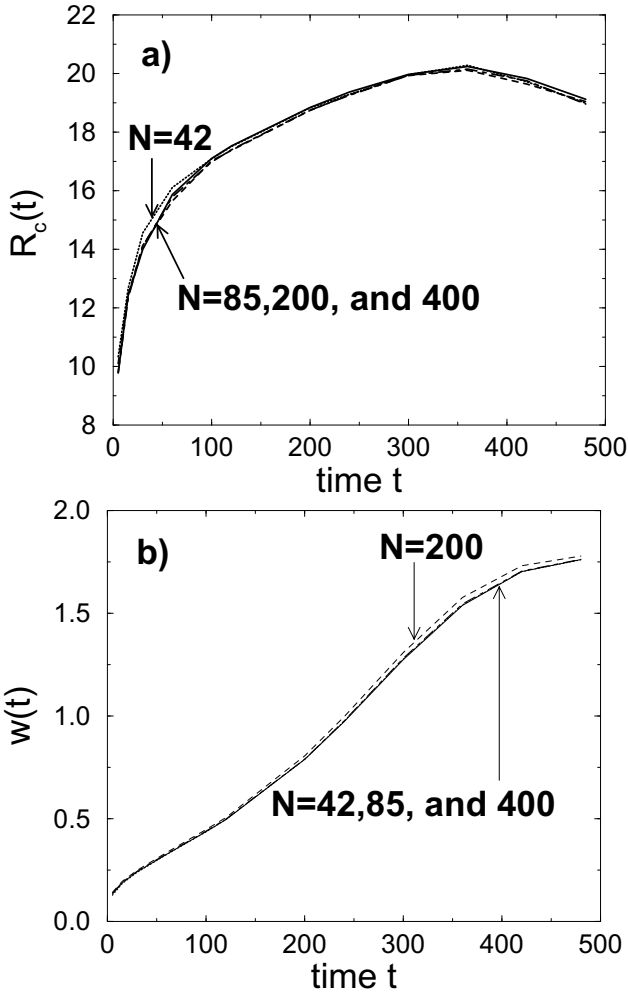

Fig. 2. Correlation length $R_c(t)$ and surface roughness $w(t)$ calculated from Eq. (4) using two different numerical methods on an interval $[0, L]^2$ of the size $L = 200$ subject to periodic boundary conditions. The parameters were $a_1 = -0.1045$, $a_2 = -0.4044$, $a_3 = -0.13$, $a_4 = 0.07$, and $D = 0.022$. The results ensuing from the finite difference method (13)–(15) with $N^2 = 200^2$ and $N^2 = 400^2$ grid points are depicted by the dashed and the dash-dotted lines, respectively. The results that were determined by the spectral Galerkin method (22)–(27), (29), (30) with $N = 42$ and $N = 85$ are represented by the dotted and the solid lines, respectively. Therefore, each part of this figure contains four different lines. As a result of the good agreement between the different simulation methods, the difference between most of these lines is not visible.

3. Spectral Galerkin method

The spectral Galerkin method is a numerical method to solve the spatial evolution of partial differential equations in Fourier space. It is especially efficient in the time interval where the linear parts of the equation dominate. For analytical and numerical results on the convergence of the spectral Galerkin method for the one-dimensional version of Eq. (4) we refer to Ref. [15]. In this paper, we focus on stochastic growth equations in two spatial dimensions. Then, Eq. (4) reads in Fourier space

$$\partial_t \tilde{h}(\vec{k},t) = \sigma(k)\tilde{h}(\vec{k},t) + (-a_3 k^2 + a_4)\tilde{v}(\vec{k},t) + \tilde{\eta}(\vec{k},t) \tag{17}$$

with

$$\sigma(k) = -a_1 k^2 + a_2 k^4 \,, \tag{18}$$

$$\tilde{h}(\vec{k},t) = \int d^2x\, h(\vec{x},t) \exp(-i\vec{k}\cdot\vec{x}) \,, \tag{19}$$

$$\tilde{v}(\vec{k},t) = \int d^2x\, [\nabla h(\vec{x},t)]^2 \exp(-i\vec{k}\cdot\vec{x}) \,, \tag{20}$$

$$\tilde{\eta}(\vec{k},t) = \int d^2x\, \eta(\vec{x},t) \exp(-i\vec{k}\cdot\vec{x}) \,. \tag{21}$$

For the time discretization usually a semi-implicit Euler scheme is applied

$$\begin{aligned} \tilde{h}^{(n+1)}(\vec{k}) &= \tilde{h}^{(n)}(\vec{k}) + \Delta t_n \sigma(k) \tilde{h}^{(n+1)}(\vec{k}) \\ &\quad + \Delta t_n (-a_3 k^2 + a_4)\tilde{v}^{(n)}(\vec{k}) + \tilde{q}^{(n)}(\vec{k}) \,, \end{aligned} \tag{22}$$

where $\tilde{h}^{(n)}(\vec{k})$, $\tilde{v}^{(n)}(\vec{k})$, and $\tilde{q}^{(n)}(\vec{k})$ are a short hand notation for $\tilde{h}(\vec{k},t_n)$, $\tilde{v}(\vec{k},t_n)$, and the noise contribution: $\tilde{q}^{(n)}(\vec{k}) = \int_{t_n}^{t_n+\Delta t_n} dt\, \tilde{\eta}(\vec{k},t)$. The wave vector $\vec{k}$ is of the form $\vec{k} = \frac{2\pi}{L}(n_x, n_y)$ with $n_x, n_y \in \mathbb{Z}$. The semi-implicit time discretization has the advantage that larger time steps Δt_n are allowed in comparison to an explicit scheme if the linear terms of Eq. (4) dominate.

The contributions $\tilde{q}^{(n)}(\vec{k})$ from the deposition noise are complex random numbers whose real and imaginary parts are up to the identities $\mathrm{Re}\ \tilde{q}^{(n)}(\vec{k}) = \mathrm{Re}\ \tilde{q}^{(n)}(-\vec{k})$ and $\mathrm{Im}\ \tilde{q}^{(n)}(\vec{k}) = -\mathrm{Im}\ \tilde{q}^{(n)}(-\vec{k})$ independent, normally distributed random numbers. Their first and second moments read

$$\langle \mathrm{Re}\ \tilde{q}^{(n)}(\vec{k}) \rangle = 0 \,, \tag{23}$$

$$\langle \mathrm{Im}\ \tilde{q}^{(n)}(\vec{k}) \rangle = 0 \,, \tag{24}$$

$$\langle [\mathrm{Re}\ \tilde{q}^{(n)}(\vec{k})][\mathrm{Re}\ \tilde{q}^{(n)}(\vec{k}')] \rangle = \begin{cases} 2D\Delta t_n L^2 & \text{if } \vec{k} = \vec{k}' = 0 \,, \\ D\Delta t_n L^2 & \text{if } \pm\vec{k} = \vec{k}' \neq 0 \,, \\ 0 & \text{otherwise} \,, \end{cases} \tag{25}$$

$$\langle[\mathrm{Re}\ \tilde{q}^{(n)}(\vec{k})][\mathrm{Im}\ \tilde{q}^{(n)}(\vec{k}')]\rangle = 0\,, \tag{26}$$

$$\langle[\mathrm{Im}\ \tilde{q}^{(n)}(\vec{k})][\mathrm{Im}\ \tilde{q}^{(n)}(\vec{k}')]\rangle = \begin{cases} D\Delta t_n L^2 & \text{if } \vec{k} = \vec{k}' \neq 0\,, \\ -D\Delta t_n L^2 & \text{if } -\vec{k} = \vec{k}' \neq 0\,, \\ 0 & \text{otherwise}\,. \end{cases} \tag{27}$$

Here, it is interesting to note that the discrete Fourier transform of the stochastic contribution to the finite difference scheme (6)

$$\tilde{q}^{(n)}_{\Delta x}(\vec{k}) = (\Delta x)^2 \sum_{j,l} P_n \xi^{(n)}_{j,l} \exp[-i(k_x j\Delta x + k_y l\Delta x)] \tag{28}$$

has the same first and second moments (23)–(27) if the wave vectors $\vec{k} = (k_x, k_y)$ are in the range $-\pi/\Delta x < k_x < \pi/\Delta x$ and $-\pi/\Delta x < k_y < \pi/\Delta x$. This also confirms that the deposition noise η has been given the correct weight in the finite difference method (6).

Equation (22) can only be solved in a finite area A of the Fourier space that consists of wave vectors $\vec{k} = \frac{2\pi}{L}(n_x, n_y)$ with $-N \leq n_x, n_y \leq N$ where N is a sufficiently large integer number. If $\vec{k}$ lies outside of the area A we set $\tilde{h}^{(n)}(\vec{k}) = 0$. Therefore, we actually compute $(2N+1)^2$ modes. It is necessary to determine the $\tilde{v}^{(n)}(\vec{k})$ from the $\tilde{h}^{(n)}(\vec{k})$. For this, we determine $\nabla h(\vec{x}, t_n)$ in real space by

$$\nabla h(\vec{x}, t_n) = \frac{1}{L^2} \sum_{\vec{k}} i\vec{k}\tilde{h}^{(n)}(\vec{k}) \exp(i\vec{k}\cdot\vec{x}) \tag{29}$$

on M^2 equidistant grid points in $[0, L]^2$ that have the distance $\Delta x = L/M$. Then, we calculate $[\nabla h(\vec{x}, t_n)]^2$ on the M^2 grid points and finally transform it back into the Fourier space:

$$\tilde{v}^{(n)}(\vec{k}) = (\Delta x)^2 \sum_{\vec{x}} [\nabla h(\vec{x}, t_n)]^2 \exp(-i\vec{k}\cdot\vec{x})\,. \tag{30}$$

Note that M must be a power of 2 because we use the fast Fourier transformation [21]. In addition, M must also fulfill the condition $M \geq 3N + 1$, in order to take care of the known "aliasing" problem. The sum $\sum_{\vec{k}}$ in Eq. (29) is restricted to wave vectors that lie inside the area A. Therefore, the sum in the relation

$$[\nabla h(\vec{x}, t_n)]^2 = \frac{1}{L^2} \sum_{\vec{k}} \tilde{v}^{(n)}(\vec{k}) \exp(i\vec{k}\cdot\vec{x}) \tag{31}$$

refers to a larger area B of wave vectors $\vec{k} = \frac{2\pi}{L}(n_x, n_y)$ with integer numbers n_x and n_y between $-2N$ and $2N$. However, two different Fourier modes with

wave vectors $\vec{k} = \frac{2\pi}{L}(n_x, n_y)$ and $\vec{k}' = \frac{2\pi}{L}(n'_x, n'_y)$ cannot be distinguished on the M^2 grid points if $n'_x - n_x$ and $n'_y - n_y$ are divisible by M. In that case the RHS of Eq. (30) would only yield the sum of their Fourier coefficients. Since we only need the coefficients $\tilde{v}^{(n)}(\vec{k})$ with $\vec{k} \in A$, it is sufficient and necessary that all Fourier modes with wave vectors in A can be distinguished from different non-vanishing Fourier modes whose wave vectors lie inside the area B. Therefore, $-N + M \geq 2N + 1$ must hold, yielding the condition $M \geq 3N + 1$. Note that in the presence of a third order nonlinearity like *e.g.* $\nabla \cdot (\nabla h)^3$ the condition $M \geq 3N+1$ had to be replaced by $M \geq 4N+1$ and that in the presence of a tenth order term like *e.g.* $(\nabla h)^{10}$ M had to fulfill the condition $M \geq 11N + 1$, and so on. On the other hand, if we had to calculate a non-polynomial nonlinearity like *e.g.* $1/\sqrt{1 + (\nabla h)^2}$, the "aliasing" of different Fourier modes could not be completely avoided. In that case, we had to rely on the damping of Fourier modes with large wave vectors $\vec{k}$ resulting from stabilizing terms like *e.g.* $a_2 \nabla^4 h$ in Eq. (4) that smooth the height profile $h(\vec{x}, t)$, so that also nonlinearities like $1/\sqrt{1 + (\nabla h)^2}$ basically consist of Fourier modes from a finite area of the Fourier space.

As a specific application, we have solved Eq. (4) using the spectral Galerkin method (22)–(27), (29), (30) and using the same parameters as in the previous section. Fig. 2 shows the resulting surface roughness $w(t)$ and correlation length $R_c(t)$ for $N = 42$ and $N = 85$. Their difference is not larger than 5.6% for t =5, 15, 30, and 60 and not larger than 0.69% for $t \in [100, 480]$. Therefore it seems that our numerical results arising from the finite difference method as well as from the spectral Galerkin method are of sufficient precision. The CPU-times required for one simulation run on the same computer were 1h 6min for the finite difference method with $N^2 = 200^2$ grid points, 1h 27min for the spectral Galerkin method with $N = 42$, 11h 29min for the finite difference method with $N^2 = 400^2$ grid points, and 37h 36min for the spectral Galerkin method with $N = 85$. As a consequence, the spectral Galerkin method appears to be computationally less efficient if high precision of the numerical solution of Eq. (4) is demanded.

4. Finite element method

In this section, we explain how the deposition noise η can be taken into consideration in a third numerical simulation method, the finite element solution of Eq. (4). To that end, Eq. (4) is decomposed into the system of equations

$$\partial_t h = \nabla^2 w + a_4 (\nabla h)^2 + \eta \,, \tag{32}$$

$$w = a_1 h + a_2 \nabla^2 h + a_3 (\nabla h)^2 \,. \tag{33}$$

These equations are multiplied with test functions Φ_i from the Sobolev space $H^1_{\rm per}([0,L]^2)$ and then integrated on $[0,L]^2$ [22]. In order to simulate the time evolution an implicit Euler scheme can be applied. The resulting computational scheme then reads

$$\begin{aligned}\int \Phi_i h^{(n+1)} &= \int \Phi_i h^{(n)} - \Delta t_n \int (\nabla \Phi_i)\cdot(\nabla w^{(n+1)}) \\ &\quad + \Delta t_n a_4 \int \Phi_i (\nabla h^{(n+1)})^2 + Z_i^{(n)}\,, \qquad (34)\\ \int \Phi_i w^{(n+1)} &= a_1 \int \Phi_i h^{(n+1)} - a_2 \int (\nabla \Phi_i)\cdot(\nabla h^{(n+1)}) \\ &\quad + a_3 \int \Phi_i (\nabla h^{(n+1)})^2, \qquad (35)\\ Z_i^{(n)} &= \int_{t_n}^{t_n+\Delta t_n} dt \int d^2x\, \Phi_i(\vec{x})\eta(\vec{x},t)\,, \qquad (36)\end{aligned}$$

where $h^{(n)}$ and $w^{(n)}$ denote the functions h and w at the time t_n. The equations (34)–(36) can actually only be solved for a finite number of linearly independent test functions $\Phi_1,\ldots,\Phi_N \in H^1_{\rm per}([0,L]^2)$. Therefore, we try to find the solutions $h^{(n+1)}$ and $w^{(n+1)}$ in the subspace V_N being spun by the functions $\Phi_1,\ldots,\Phi_N$.

In order to find the test functions $\Phi_1,\ldots,\Phi_N$ we subdivide the area $[0,L]^2$ into triangles. The triangulation complies with the periodic boundary conditions and the following rules. Two different triangles should share either one edge or one corner or not a single point. Two mesh points of the triangulation should not be connected by more than one edge. The test functions Φ_i are defined by the properties, that *(i)* they are continuous functions on $[0,L]^2$ and fulfill periodic boundary conditions, *(ii)* they are linear functions on each triangle, and *(iii)* that Φ_i assumes the value 1 at the mesh point P_i and the value 0 at all other mesh points P_k. As a result of this definition, Φ_i differs from zero only on the triangles that surround the mesh point P_i.

Before one can solve the system of the equations (34)–(35), the random numbers $Z_i^{(n)}$ have to be generated. These random numbers are normally distributed and have the moments

$$\begin{aligned}\left\langle Z_i^{(n)} \right\rangle &= 0, \qquad (37)\\ \left\langle Z_i^{(n)} Z_k^{(n)} \right\rangle &= 2D\Delta t_n \int \Phi_i \Phi_k \qquad (38)\end{aligned}$$

for all $i,k = 1,\ldots,N$. This yields in case $i = k$

$$\left\langle \left(Z_i^{(n)}\right)^2 \right\rangle = 2D\Delta t_n \frac{1}{6} \sum_{ii} A_\Delta \,, \tag{39}$$

where $\sum_{ii} A_\Delta$ denotes the sum of the areas of the triangles that surround the mesh point P_i. If $i \neq k$, but P_i and P_k are neighbouring points, *i.e.* they are connected by a triangle edge, Eq. (38) yields

$$\left\langle Z_i^{(n)} Z_k^{(n)} \right\rangle = 2D\Delta t_n \frac{1}{12} \sum_{ik} A_\Delta \,, \tag{40}$$

where $\sum_{ik} A_\Delta$ denotes the sum of the areas of the two triangles that have one corner in P_i and one corner in P_k. If $i \neq k$, and P_i and P_k are not neighbouring points, Eq. (38) yields

$$\left\langle Z_i^{(n)} Z_k^{(n)} \right\rangle = 0 \,. \tag{41}$$

In order to get such random numbers, one can generate for each triangle edge $\overline{P_i P_k}$ an independent, normally distributed random number $Y_{ik}^{(n)}$, that possesses the moments

$$\left\langle Y_{ik}^{(n)} \right\rangle = 0 \,, \tag{42}$$

$$\left\langle \left(Y_{ik}^{(n)}\right)^2 \right\rangle = 2D\Delta t_n \frac{1}{12} \sum_{ik} A_\Delta \,. \tag{43}$$

Then the random numbers $Z_i^{(n)}$ can be determined by [23]

$$Z_i^{(n)} = \sum_{P_k \neq P_i \text{ is a neighbouring point of } P_i} Y_{ik}^{(n)} \,. \tag{44}$$

An alternative possibility to get the random numbers $Z_i^{(n)}$ is to generate for each mesh point P_i an independent, normally distributed random number $\tilde{Z}_i^{(n)}$ and for each triangle $\overline{P_i P_k P_l}$ an independent, normally distributed random number $X_{ikl}^{(n)}$, that have the moments

$$\left\langle \tilde{Z}_i^{(n)} \right\rangle = 0 \,, \tag{45}$$

$$\left\langle \left(\tilde{Z}_i^{(n)}\right)^2 \right\rangle = 2D\Delta t_n \frac{1}{12} \sum_{ii} A_\Delta \,, \tag{46}$$

$$\left\langle X_{ikl}^{(n)} \right\rangle = 0 \,, \tag{47}$$

$$\left\langle \left(X_{ikl}^{(n)}\right)^2 \right\rangle = 2D\Delta t_n \frac{1}{12} A_{ikl} \,, \tag{48}$$

where A_{ikl} is the area of the triangle $\overline{P_iP_kP_l}$. Then the random numbers $Z_i^{(n)}$ can be calculated by

$$Z_i^{(n)} = \tilde{Z}_i^{(n)} + \sum_{\overline{P_iP_kP_l} \text{ has one corner in } P_i} X_{ikl}^{(n)} . \tag{49}$$

Since the number of triangle edges is equal to the number of mesh points plus the number of triangles in $[0, L]^2$ (because the periodic boundary conditions are considered), the two alternatives (42)–(44) and (45)–(49) require the same number of independent random numbers and therefore have the same efficiency.

5. Conclusions

In this paper we have presented a detailed account of three different numerical simulation methods for the solution of a stochastic field equation for amorphous thin film growth. We have shown, that the finite difference method and the spectral Galerkin method yield the same surface roughness $w(t)$ and the same correlation length $R_c(t)$ and that these two methods practically have the same accuracy and efficiency. It remains to show, that also the method using finite element approximations yields the same results. A further mathematical challenge presents the lack of rigorous proofs of the convergence of the different numerical approximations of Eq. (4) and even a mathematical proof of existence of a solution of Eq. (4) in the two-dimensional case.

This work has been supported by the DFG-Sonderforschungsbereich 438 München/Augsburg, TP A1. We thank E. Nash for helpful discussions and an introduction to the non-stochastic Galerkin and finite element methods.

REFERENCES

[1] A.L. Barabasi, H.E. Stanley, *Fractal Concepts in Surface Growth*, Cambridge University Press, Cambridge, UK 1995; W.M. Tong, R.S. Williams, *Annu. Rev. Phys. Chem.* **45**, 401 (1994); J. Krug, *Adv. Phys.* **46**, 139 (1997); M. Marsili, A. Maritan, F. Toigo, J.R. Banavar, *Rev. Mod. Phys.* **68**, 963 (1996).

[2] D.E. Wolf, J. Villain, *Europhys. Lett.* **13**, 389 (1990).

[3] J. Villain, *J. Phys. I* **1**, 19 (1991).

[4] S. Das Sarma, P. Tamborenea, *Phys. Rev. Lett.* **66**, 325 (1991).

[5] Z.-W. Lai, S. Das Sarma, *Phys. Rev. Lett.* **66**, 2348 (1991).

[6] M. Siegert, M. Plischke, *Phys. Rev.* **E50**, 917 (1994).

[7] B. Reinker, M. Moske, K. Samwer, *Phys. Rev.* **B56**, 9887 (1997).

[8] S.G. Mayr, M. Moske, K. Samwer, *Mater. Sci. Forum* **343-346**, 221 (2000).

[9] S.G. Mayr, M. Moske, K. Samwer, *The Growth of Vapor Deposited Amorphous ZrAlCu-Alloy Films: Experiment and Simulation*, in H.-J. Bungartz, R.H.W. Hoppe, C. Zenger: *Lectures on Applied Mathematics*, 2000, p. 233.

[10] T. Salditt, T.H. Metzger, J. Peisl, B. Reinker, M. Moske, K. Samwer, *Europhys. Lett.* **32**, 331 (1995).

[11] M. Raible, S.G. Mayr, S.J. Linz, M. Moske, P. Hänggi, K. Samwer, *Europhys. Lett.* **50**, 61 (2000).

[12] M. Raible, S.J. Linz, P. Hänggi, *Phys. Rev.* **E62**, 1691 (2000).

[13] M. Raible, S.J. Linz, P. Hänggi, *Phys. Rev.* **E64**, 31506 (2001).

[14] M. Moske, *Mechanische Spannungen als Sonde für Schichtwachstum und Schichtreaktionen*, Habilitationsschrift, Universität Augsburg, 1997.

[15] D. Blömker, C. Gugg, M. Raible, *Thin-Film-Growth-Models: Roughness and Correlation Functions*, *Europ. J. Appl. Math.*, in press 2002.

[16] K. Moser, J. Kertész, D.E. Wolf, *Physica A* **178**, 215 (1991).

[17] J.G. Amar, F. Family, *Phys. Rev.* **A41**, 3399 (1990).

[18] C.-H. Lam, F.G. Shin, *Phys. Rev.* **E58**, 5592 (1998).

[19] M. Kardar, G. Parisi, Y.-C. Zhang, *Phys. Rev. Lett.* **56**, 889 (1986).

[20] P.E. Kloeden, E. Platen, H. Schurz, *Numerical Solution of SDE Through Computer Experiments*, Springer-Verlag, Berlin, Heidelberg 1994.

[21] W.H. Press, S.A. Teukolsky, W.T. Vetterling, and B.P. Flannery, *Numerical Recipes in C*, Cambridge University Press, Cambridge, UK 1992.

[22] C. Großmann, H.-G. Roos, *Numerik partieller Differentialgleichungen*, B.G. Teubner, Stuttgart 1992.

[23] M. Raible, *Stochastische Feldgleichungen für amorphes Schichtwachstum*, Dissertation, Universität Augsburg, Shaker Verlag, Aachen 2000.